PAPER

Check for updates

Thermo-catalytic decomposition of cotton seed press cake over nickel doped zeolite Y, hydrogen: enhanced yield of bio-oil with highly selective fuel-range hydrocarbons†

Marrij Afraz,[a] Jan Nisar, *[a] Afzal Shah, *[b] Ghulam Ali,[a] Faisal Muhammad,[a] Farooq Anwar*[cd] and Wan Azlina Wan Abdul Karim Ghani[e]

This research reports the yield of bio-oil from cotton seed press cake (CSPC) *via* an optimized thermo-catalytic pyrolysis using nickel impregnated zeolite Y, hydrogen catalyst. The catalyst, raw biomass and catalyst impregnated biomass were characterized using different analytical techniques. The ideal temperature, duration, and catalyst concentration for pyrolysis experiments were determined to be 300 °C, 20 minutes, and 5% of Ni-doped zeolite Y, hydrogen, respectively, in order to achieve the best bio-oil yield (35%). Gas chromatography-mass spectrometry (GC-MS) of pyrolytic bio-oil depicted the presence of C_2-C_{26} hydrocarbons. The findings of this investigation showed that the synthesis of bio-oil with highly selective fuel-range hydrocarbons could be efficiently induced through the pyrolysis of CSPC biomass employing nickel impregnated zeolite Y, hydrogen catalyst. Moreover, thermogravimetric analysis (TGA) of cotton seed press cake with catalyst was carried out at various heating rates to find out the kinetic parameters. Employing Kissinger model, activation energy (E_a) and frequency factor (A) for various components of biomass *i.e.*, hemicellulose, cellulose and lignin were calculated as 83.14 kJ mol^{-1}, 99.76 kJ mol^{-1}, 124.71 kJ mol^{-1} and 1.9×10^7 min^{-1}, 1.0×10^8 min^{-1}, 1.0×10^{10} min^{-1}, respectively. It can be concluded from the results that cotton seed press cake waste has potential for use as a pyrolysis feedstock in large-scale bio-fuel production.

1. Introduction

Energy stability is the desired sustainable development goal (SDG) of any developing nation; however, both developing and non-developing countries are facing energy crises.[1] The reduction in fossil fuel resources is the result of their maximal utilization.[2] In addition, the use of fossil fuels leads to grave environmental consequences.[3] Therefore, the adoption of renewable energy sources is important climate change reversal practice because it can lessen our reliance on non-renewable energy sources for environmental protection.[4] Massive amounts of biomass waste are produced globally but not fully utilized.[5] Limiting the use of fossil fuels and switching to fuel with low carbon levels for energy can help reduce the emission of greenhouse gases.[6] The advancement of bioenergy is a promising substitute for meeting the growing demand of energy and can prove a sustainable supply for the economies of emerging countries.[7]

With this consideration, researchers have now focused on using biomass to produce biofuels, which could serve as a reliable and safer alternative to fossil fuels for energy production.[8,9] Pakistan, an agricultural country, generates a lot of biomass waste that is wasted while it could be used to make biofuels through pyrolysis and other conversion processes.[10] At very high temperature and in oxygen-poor environment, biomass decomposition yields bio-oil, biochar, and gaseous volatile compounds.[11,12] The most popular conversion technique is thought to be fast pyrolysis because of its many benefits, such as lower cost, minimal emissions of CO_2, SO_X, and NO_X, improved thermal efficiency, and a high calorific value.[13] Given that a substantial volume of bio-oil is produced as this is the most effective way to transform biomass into valuable products.[14] However, the quality of the bio-oil is degraded during pyrolysis by a number of oxygenated chemicals that are formed.

aNational Centre of Excellence in Physical Chemistry, University of Peshawar, Peshawar 25120, Pakistan. E-mail: jan_nisar@uop.edu.pk; marijafrazkhan210@gmail.com; ghulamali@uop.edu.pk; faisalmuhammad77318@gmail.com

bDepartment of Chemistry, Quaid-i-Azam University, Islamabad 45320, Pakistan. E-mail: afzals_qau@yahoo.com

cDepartment of Food Science, Faculty of Food Science and Technology, Universiti Putra Malaysia, 43400 UPM Serdang, Selangor, Malaysia

dInstitute of Chemistry, University of Sargodha, Sargodha, 40100, Pakistan. E-mail: fqanwar@yahoo.com

eDepartment of Chemical and Environmental Engineering, Sustainable Process Engineering Research Centre (SPERC), Universiti Putra Malaysia, 43400 Serdang, Selangor, Malaysia. E-mail: wanazlina@upm.edu.my

† Electronic supplementary information (ESI) available. See DOI: https://doi.org/10.1039/d4ra06163b

Therefore, researchers are keen to enhance the quality of bio-oil by testing specific catalysts to convert oxygenated pollutants into useable hydrocarbons.[15,16]

Zeolite is a crystalline nano-porous material with large surface area that is widely used as a catalyst in oil processing industry.[17] Silica and alumina based zeolites with high porosity are more in demand for adsorption and processing of heavy molecules; however, their synthesis is quite difficult and time consuming.[18,19] Using metal impregnation over zeolite, during pyrolysis is a potential method to produce highly selective hydrocarbons in the bio-oil. The metal impregnation changes the acidic character of the zeolite and produces pyrolysates that are incredibly selective. Prior to 1980 Brønsted acidic zeolites were considered to play a key role in cracking the biomass, however, the discovery of Ti-silicalite-1 in 1983 established the presence of isolated tetrahedral Ti-specie, replacing Si-atom in the zeolite which led to Lewis acid sites and the development and utilization of Lewis acid zeolite catalyst took a better role in the bio-based chemistry.[20] The low concentration of Brønsted acid sites in the parental zeolite and the high concentration of Lewis sites in the freshly doped metal reduce the amount of surplus bio-oil cracking and lead to a favorable yield of monocyclic aromatic hydrocarbons. The acidity of the catalyst increases the effectiveness of the metal impregnation on it when compared to the porous nature of the parent catalyst.[16,21] Widayatno et al.,[22] upgraded bio-oil from pyrolysis of biomass over Cu-modified β-zeolite. They observed that when β-zeolite was modified with a small amount of 0.50 wt% of Cu, the selectivity improved as compared to parent zeolite and maintained its activity for numerous reuses without regeneration. The lesser Cu loading on β-zeolite increased the surface area and formation of more micropores. However, in case of more loaded Cu, the selectivity decreased as the surface area increased to maximum at 0.50 wt% of Cu doping. At 1.00 wt%, copper species aggregated on surface of zeolite, leading to obstruction of zeolite pores and diminishing the surface area. Therefore, proper loading amount of metal on zeolite is very important for getting positive results.

Furthermore, a significant amount of high-quality organic waste is produced by farming and agro-processing operations, such as rice husk, sugar cane bagasse, cotton and corn stalks, cotton seed press cakes, and fruit shells, among others, and they can be utilized for generating affordable energy.[23] One of the plants, *Gossypium hirsutum* L., frequently referred to as cotton, is the most extensively grown and historically recognized seed crop.[24] Owing to its high productivity worldwide, cotton generates a lot of trash in the form of cottonseed press cake, cotton stalks, and other waste products. Cotton seed provides 17.7% of Pakistan's edible oil needs, and once oil is extracted, a significant amount of residue is produced in the form of cake.[25] This residue is dumped as waste, which can be used to produce fuel using an appropriate method.[24]

The primary emphasis of this work is to investigate the kinetics of the breakdown process by pyrolyzing cotton seed press cake using Ni-doped zeolite Y, hydrogen as catalyst. Another aim of this study is to examine the impacts of various parameters, including temperature, time, and catalyst concentration, on the yield and quality of pyrolysis products/bio oil of cotton seed press cake.

2. Experimental

2.1. Material

Cotton seed press cake used in this experiment was obtained from an oil extraction unit in Southern Punjab. The remaining oil from the seed press cake was extracted through *n*-hexane using a Soxhlet apparatus. 100 g of powdered press cake was fed into Soxhlet assembly fitted on heating mantle and extraction was run in the presence of *n*-hexane (b.p. 65–68 °C) as extracting solvent for almost 4–5 hours. After that, the press cake was dried for roughly 20 days in the shade. After being ground into powder with the help of an electrical crusher, the sample was sieved through a mesh size of 35 and kept in plastic bags to avoid moisture absorption or addition of any other contaminants. Zeolite Y, hydrogen with a $SiO_2 : Al_2O_3$ molar ratio of 80 : 1 was obtained from Alfa Aesar, Germany. Nickel sulphate hexahydrate was procured from Sigma-Aldrich. The flasks and condenser used were washed by acetone after being used in the experiment.

2.2. Preparation of Ni-doped zeolite Y, hydrogen

Wet impregnation method was used to dope nickel onto the parent catalyst by dissolving 14.58 g of zeolite Y, hydrogen and 2.62 g of nickel sulphate hexahydrate in 100 mL of distilled water and stirred for one hour using a magnetic stirrer. In order to keep the pH of the solution at 9, NaOH was added dropwise at regular intervals. After precipitation, the filtrate obtained was thoroughly rinsed with water multiple times until the pH reached 7. Then it was put in oven at 110 °C for 12 h and afterwards calcined at 550 °C for 5 h and 30 min.

2.3. Characterization of catalyst and biomass

The morphology of Ni-doped zeolite Y, hydrogen, raw and catalyst impregnated biomass samples was determined *via* SEM (JSM-5910 JEOL Japan). The sample was coated with gold for assuring conductivity and put on sample stub. The instrument was set to take SEM micrograph. Elemental analysis was done through Electron dispersive X-ray analyzer interfaced with scanning electron microscope (INCA200/Oxford instruments, UK). This instrument was used to study the catalyst, raw and catalyst impregnated biomass samples for the determination of atomic and weight percentages of elements present in cotton-seed cake and catalyst. The resulting signals provided a distinctive X-ray patterns corresponding to the identified elements. Crystallinity and amorphousness of Ni-doped zeolite Y, hydrogen were assessed using XRD (JDX-3532 JEOL Japan) with Cuka (wavelength 1.5418 Å). The sample's crystalline size was measured within 2θ-ranges of 0 to 160°.

2.4. Pyrolysis

The pyrolysis experiments of cotton seed press cake with Ni-doped zeolite Y, hydrogen were performed in pyrolysis apparatus (Fig. 1) demonstrated in detail in our previous article.[26] Prior to the actual experiment, the conditions for sample preparation and equipment were equilibrated. For performing each experiment, 5 g of sample with 5% Ni-doped zeolite Y,
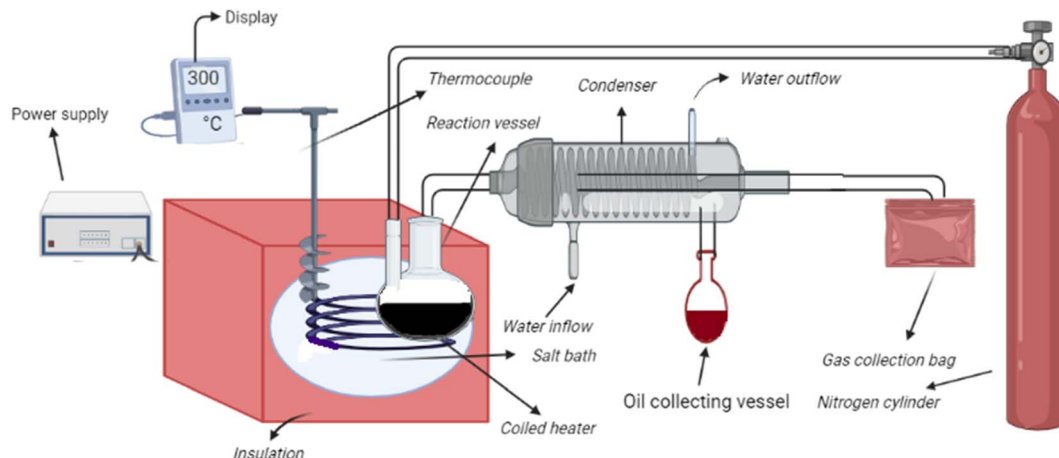
Fig. 1 Pyrolytic system.

hydrogen was taken in a Pyrex flask and placed in the pyrolysis chamber at desired temperature. The flask was attached to a condenser. Experiments were performed in nitrogen gas flow of 150 mL min^{-1} at temperature ranging from 280 to 340 °C. A controller was used to maintain temperature through a K-type thermocouple. The liquid fraction obtained from thermocatalytic pyrolysis of cotton seed press cake was studied using GCMS. Helium was employed as carrier gas at a split ratio of 1 : 18 and at a flow rate of 2.0 mL min^{-1}. A volume of around 1 μL was inserted to the injection port at 60 °C and holding time of 1 minute. Afterwards the temperature was raised to 265 °C at 4 °C min^{-1} followed by holding period of 5 minutes. Agilent HP-5 was the column utilized for analysis. The NIST-05 library of GC-MS was then used to evaluate and identify the GC-MS chromatograph's peak results.

2.5. Kinetic study

Thermogravimetric analysis was performed through a Q500 thermogravimetric analyzer. The sample was decomposed in thermogravimetric analyzer at heating rates of 5, 10, 15 and 20 °C min^{-1} in the temperature range from 25 to 800 °C. Activation energy and frequency factor were determined using Kissinger equation (eqn (1)).[27]

$$\ln\left[\frac{\beta}{T_m^2}\right] = \ln\left(\frac{AR}{E_a}\right) - \frac{E_a}{RT_m} \tag{1}$$

where E_a, A, β and T_m represent activation energy, frequency factor, heating rate and maximum degradation temperature.

3. Results and discussion

3.1. Characterization of catalyst

SEM was used to examine the morphological properties of both zeolite Y, hydrogen and nickel doped zeolite Y, hydrogen (shown in Fig. 2a and b). Nickel doping on the zeolite Y, hydrogen resulted in the presence of aggregated polyhedral and cubic-shaped particles surrounded by a significant number of highly aggregated particles. As shown in Fig. 2b, nickel is coupled to the zeolite Y, hydrogen making clusters, and the loading of nickel on zeolite Y, hydrogen results in an increase in
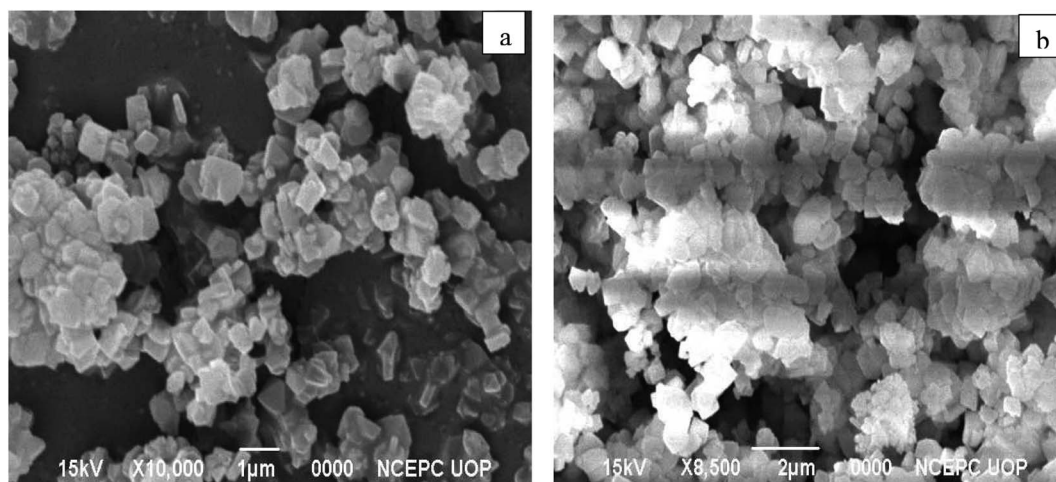

Fig. 2 (a) SEM of zeolite Y, hydrogen (b) SEM of Ni impregnated zeolite Y, hydrogen.

grain diameter, indicating an even distribution of nickel on zeolite. Our research strategy corresponds to past findings. Xu et al.[28] investigated the morphology of nickel-impregnated zeolite and found nickel dispersion on zeolite grains, resulting in agglomeration and the development of agglomerates. This observation clearly demonstrates the doped zeolite's highly crystalline character. According to Uddin et al.'s SEM study of the zeolite,[29] polyhedral structures allowed the particles to be found either as single crystallites or as clusters of distinct crystals.

The elemental distribution of nickel on the surface of the nickel doped catalyst was studied using EDX. Fig. 3 shows that oxygen (51.14%), silicon (28.85%), aluminum (8.2%), carbon (9.61%), and nickel (2.20%) are present. These findings are consistent with those of previously reported investigations. Kalhor and Zarnegar[30] used EDX to analyze the elemental composition of nickel loaded zeolite and discovered the existence of aluminum, silicon, carbon, nickel, oxygen, and sodium etc., in the synthesized sample. In another study Kalhor and Zarnegar[31] also observed Si, Al, Ni, O, and Na in nickel-doped zeolite using EDX.

The crystallinity of zeolite Y, hydrogen and nickel-doped zeolite Y, hydrogen was determined by XRD. The XRD of both the samples are shown in Fig. 4a and b. Peaks of various intensities were observed at different 2θ values ranging from 10 to 160°. A clear difference can be observed between the two XRD images. The doping of nickel on zeolite Y, hydrogen has an imminent effect vis-a-vis increase in intensity and sharpness of peaks as compared to undoped zeolite which showed the highly crystalline nature of the sample. The crystallite size increased due to nickel loading on zeolite Y, hydrogen. The crystallite size of Ni loaded zeolite was calculated using Scherrer equation, and found to be 0.34 nm as compared to 0.16 nm for undoped zeolite Y hydrogen. Malyala et al.[32] conducted XRD of nickel loaded zeolite and observed increase in intensity of peaks as compared to undoped zeolite which showed the highly crystalline nature of
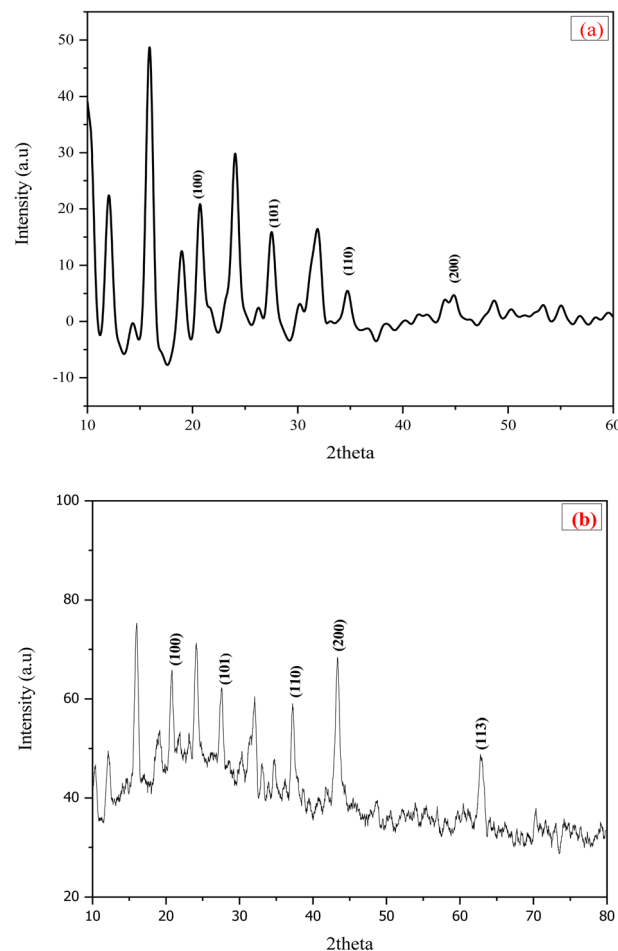
Fig. 4 (a) XRD of zeolite Y, hydrogen (b) XRD of Ni impregnated zeolite Y, hydrogen.

the sample. Philipus et al.[33] carried out the XRD of Ni-supported zeolite and identified no unwanted peaks other than those associated with doped material. Applying Scherrer equation, the
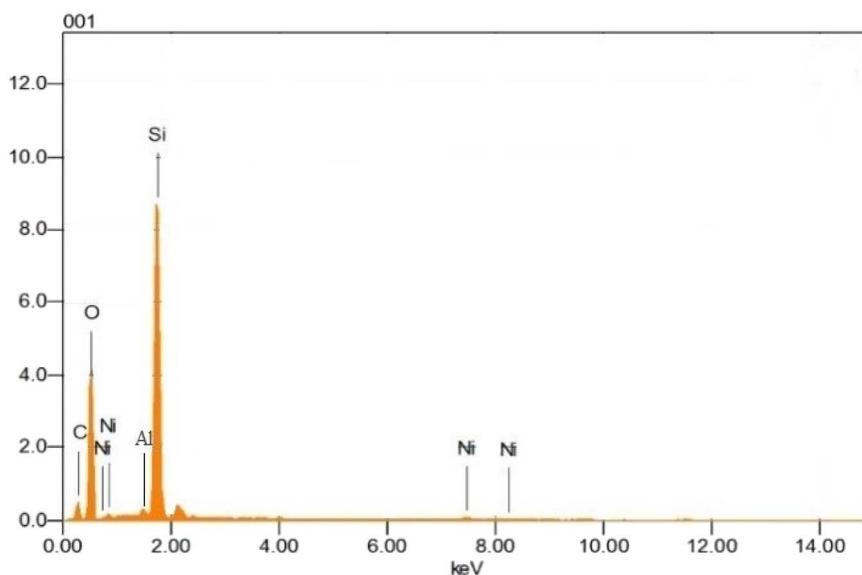
Fig. 3 EDX of Ni impregnated zeolite Y, hydrogen.

mean crystallite size was observed almost 0.27 nm. This conclusion is in conformity with our study.

3.2. Characterization of biomass

The structural examination of raw cotton seed press cake was performed using SEM images that revealed its porous structure, as shown in Fig. 5a. The raw biomass was shown to have disorganized clusters with spongy pores. The detected pores had an uneven particle size distribution, closed-off microstructures, and irregular and porous surfaces. Cotton seed cake particle size was measured to be 16 nm, with irregular and spheroidal shaped particles. The particles varied in size and form as well. Some particles were small, while others were large.

The morphology of biomass loaded with nickel doped zeolite was examined by SEM (Fig. 5b), and it was discovered that the pore size gradually increased after the loading of doped zeolite on biomass. It was projected that an uneven surface with high particle size, holes dispersed over the surface, and a well-developed pore structure existed. The metal-supported catalyst was found to be equally distributed throughout the biomass. These investigations are in consonant with previous research.

Thirugnanasambandham and Sivakumar[34] examined cottonseed press cake after copper was deposited on it using SEM and discovered that cottonseed meal had an extremely porous surface structure. He et al.[35] employed SEM to investigate the structural morphology of different cottonseed byproducts, revealing the existence of spongy pores and an uneven distribution of particle size. The particle dispersion was found to be non-homogeneous. Kaewpanha et al.[36] performed SEM investigation on seaweed loaded with various metals such as iron, nickel, and rhodium loaded on catalyst and discovered homogeneity in catalyst distribution over biomass. After successfully loading on biomass, the macroporous structure was determined, and a velvet-like appearance of the sample was seen when studied for nickel.

Fig. 5c depicts the elemental analysis of cotton seed press cake, which shows the occurrence of elements such as carbon, oxygen, magnesium, phosphorus, potassium, calcium, and niobium at mass percentages of 49.40%, 42.34%, 1.70%, 1.70%, 2.11%, 0.89%, and 1.85%. Following the effective impregnation of metal-loaded zeolite on biomass, the difference in its elemental contents was investigated (Fig. 5d). Carbon, oxygen, magnesium, aluminum, silica, phosphorus, potassium,
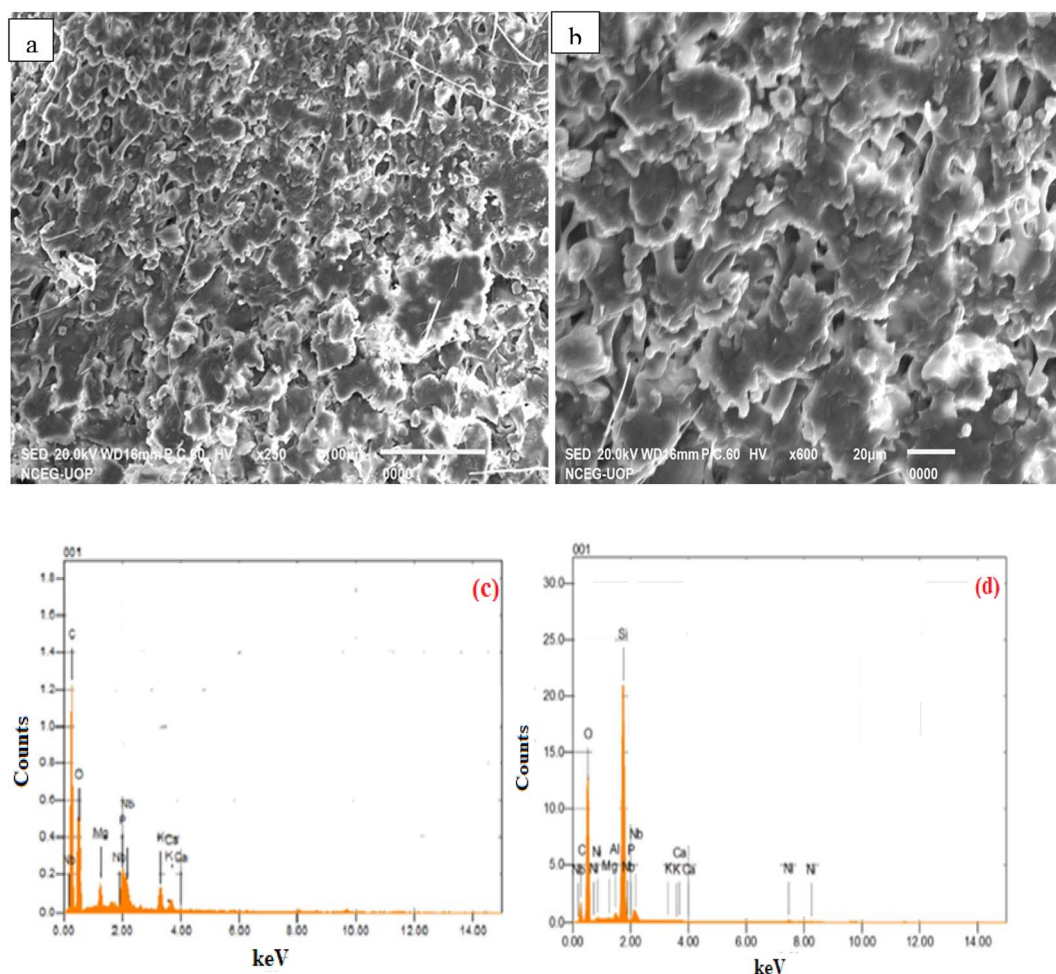

Fig. 5 (a) SEM of raw biomass (b) SEM of Ni-doped zeolite Y, hydrogen loaded biomass (c) EDX of raw biomass (d) EDX of Ni-doped zeolite Y, hydrogen loaded biomass.

calcium, nickel, and niobium were found with varied mass percentages of 26.16%, 58.43%, 0.16%, 0.13%, 13.63%, 0.48%, 0.02%, 0.06%, 0.37%, and 0.56%. These findings are consistent with previous study. For example, Sankari et al.[37] investigated the elemental composition of cottonseed press cake and discovered significant levels of Cu, Fe, Mn, P, K, and Ca, as well as moisture and several volatile chemicals. Volli and Singh[38] investigated the elemental composition of cottonseed press cake and observed trace levels of numerous chemical compounds as well as carbon (52%), oxygen (41%), nitrogen (1.3%), and sulfur (0.61%).

3.3. Pyrolysis of cotton seed press cake and optimization of various parameters

A locally constructed furnace was utilized to conduct pyrolytic experiments on cotton seed press cake with Ni-doped zeolite Y, hydrogen throughout a range of time and temperature. Our first goal was to see the influence of temperature on pyrolysates yield. Second, time was optimized while keeping the temperature constant. Temperature has the greatest influence on the yield of pyrolytic products. Fig. 6a shows temperature optimization with the oil content gradually increasing by raising the temperature from 280 to 300 °C and then gradually decreasing with increase in temperature. The decrease in amount of bio-oil at high temperature was ascribed to greater degradation at elevated temperature which amplified the gas yield. Another reason for lesser yield of bio-oil at high temperature is the secondary decomposition of oil into non-condensable products at high temperature. The conclusions derived in this work are in conformity with reported observations of Gonzalez et al.[39] and Faisal et al.[40] As a result, the optimal temperature for oil content in the presence of Ni-doped zeolite Y, hydrogen was determined to be 300 °C. As shown in Fig. 6b, time optimization revealed that the best degradation time at optimized temperature for the sample with Ni-doped catalyst was 20 minutes. To examine the influence of catalyst on pyrolysate yield, experiments were done by mixing samples with varying amounts of catalyst (1%, 2%, 3%, 4%, 5%, 6%, and 7%) at optimal time and temperature. As illustrated in Fig. 6c, a content of 5% of Ni-doped zeolite Y, hydrogen resulted in a maximum bio-oil yield of 35%. Statistical tests confirming the significance of the observed differences in bio-oil yields under various conditions are given in ESI in Tables S1–S3.†

3.4. Characterization of bio-oil

GC-MS was used to analyze the bio-oil collected at optimal temperature. A GC-MS chromatogram of the bio-oil is depicted in Fig. S1 in ESI,† whereas the compounds detected in the chromatogram are shown in Table 1. The oil produced under optimum conditions revealed that it is a mixture of aliphatic and aromatic hydrocarbons, some of which have properties appropriate for usage as fuels. Major components obtained from bio-oil breakdown were benzene derivatives, phenols, vinyl furan, formic acid, succinic acid, catechol, pyridinol, triallylsilane and various other aromatics. The main alkanes with significant abundance are cyclohexane (1,1,2-trimethyl-),
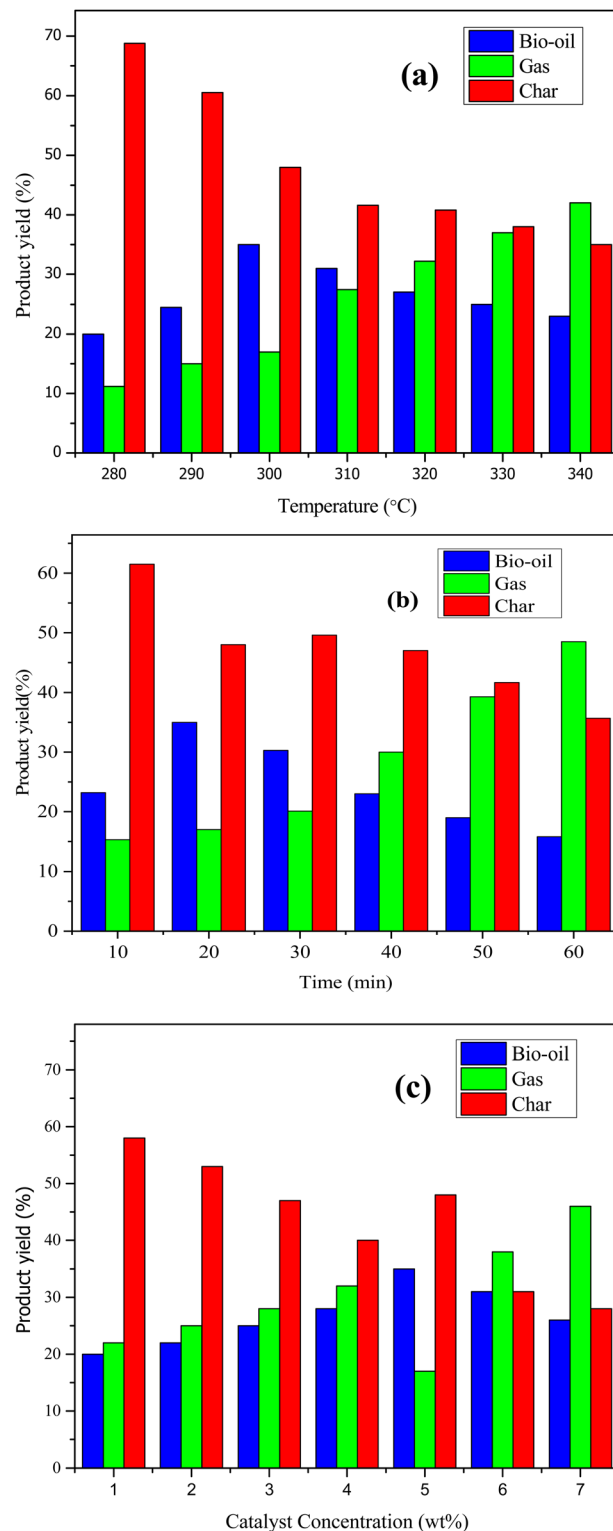

Fig. 6 (a) Temperature optimization (b) time optimization (c) catalyst optimization.

cyclohexane (1,1,3,5-tetramethyl), cyclohexane (1-ethyl-2-propyl-), and 1,3-dimethyl-5-isobutylcyclohexane. The main alkenes detected include 1,2-dihydro-3-phenylnaphthalene, 5-ethyl-1-nonene, 2-hexene (2-methyl-) and 3-heptene (2,2,3,5,6-

Table 1 Composition of oil as identified by GCMS

S. no.	Ret/time	Compounds	Chem. formula	Mol. wt. (g mol^{-1})	Area (%)
1.	3.14	Tetramethylammonium perchlorate	$C_8H_{20}N\cdot ClO_4$	229.70	0.80
2.	3.24	Acetamide	CH_3CONH_2	59.07	0.45
3.	3.33	*N,N*-Dimethylacetamide	C_4H_9NO	87.12	0.25
4.	3.51	Benzene-D6	C_6D_6	84.16	1.67
5.	3.61	Urea, trimethyl-	$C_4H_{10}N_2O$	102.14	0.15
6.	3.69	Isocrotonic acid	$C_4H_6O_2$	86.09	0.51
7.	3.86	Methyl isobutyl ketone	$(CH_3)_2CHCH_2COCH_3$	100.16	0.16
8.	3.69	Piperazine, 1-methyl-	$C_5H_{12}N_2$	100.16	0.28
9.	4.09	1*H*-Imidazole, 1-methyl-	$C_4H_6N_2$	82.10	0.06
10.	4.30	Oxirane, 2-methyl-2-pentyl-	$C_6H_{12}O$	100.15	0.15
11.	4.37	2-Vinylfuran	C_6H_6O	94.11	0.36
12.	4.46	Phenol	C_6H_6O	94.19	0.19
13.	4.56	1,3-Benzenediamine, 4-methyl-	$C_7H_{10}N_2$	122.16	0.20
14.	4.64	Formic acid phenyl ester	$C_7H_6O_2$	122.12	0.33
15.	4.73	Cyclohexanone, 2-propyl-	$C_9H_{16}O$	140.2	0.09
16.	4.78	2,4-Dimethyl-2-oxazoline-4-methanol	$C_6H_{11}NO$	129.15	0.34
17.	4.09	1*H*-Pyrazole, 1,3-dimethyl-	$C_5H_8N_2$	96.13	0.56
18.	5.02	2-Hexene, 2-methyl-	C_7H_{14}	98.19	0.42
19.	5.07	2-Aminopyridine	$C_5H_6N_2$	94.11	0.16
20.	5.19	1,2-Cyclopentanedione, 3-methyl-	$C_6H_8O_2$	112.1	1.28
21.	5.54	2,5-Pyrrolidinedione, 1-methyl-	$C_5H_7NO_2$	113.11	0.53
22.	5.63	2-Amino-4-methylpyrimidine	$C_5H_7N_3$	109.13	0.17
23.	5.81	Phenol, 2-methoxy-	C_7H_8O	122.13	3.15
24.	5.95	1-Methyl-2,4,5-trioxoimidazolidine	$C_4H_4N_2O_3$	128.09	0.44
25.	5.98	Ether, 3-butenyl pentyl	$C_9H_{18}O$	142.24	0.86
26.	6.22	Butanoic acid, 2-propenyl ester	$C_7H_{12}O$	128.16	0.30
27.	6.36	Hydrazine, (3-fluorophenyl)-	$C_6H_7FN_2$	126.13	0.65
28.	6.43	2-Butanone, 4-hydroxy-3-methyl-	$C_5H_{10}O$	102.13	0.69
29.	6.59	1,2,3-Propanetriol, 1-acetate	$C_5H_{10}O_4$	134.13	1.24
30.	6.62	1-Propanol, 3-chloro-, acetate	$C_5H_9ClO_2$	136.58	0.76
31.	6.79	Pyrrolidine-2,4-dione	$C_4H_5NO_2$	99.09	1.75
32.	6.85	5,6-Dihydro-6-methyluracil	$C_5H_8N_2O_2$	128.12	0.64
33.	6.92	5-Amino-3-methyl-1,2,4-oxadiazole	$C_3H_5N_3O$	99.09	3.25
34.	7.09	1,2,4-Triazine-3,5(2*H*,4*H*)-dione	$C_3H_3N_3O_2$	113.07	0.85
35.	7.22	3-Pyridinol	C_5H_5NO	95.09	1.90
36.	7.64	Propanoic acid, 2-(hydroxyimino)	$C_3H_5NO_3$	103.7	1.52
37.	7.67	Oxirane, 2-methyl-2-pentyl-	$C_8H_{16}O$	128.21	1.58
38.	8.01	Catechol	$C_6H_6O_2$	110.1	1.71
39.	8.43	1,2-Benzenediol, 3-methoxy-	C_7H_8O	140.1	1.39
40.	8.79	Benzeneacetic acid	$C_9H_{10}BrNO$	136.1	1.31
41.	8.92	2-Methoxy-4-vinylphenol	$C_9H_{10}O_2$	150.1	0.24
42.	9.09	Cyclohexanone, 2-propyl-	$C_9H_{16}O$	140.2	0.29
43.	9.32	Phenol, 2,6-dimethoxy-	$C_8H_{10}O$	154.1	0.92
44.	9.56	Pyrrole-2-carboxamide	$C_5H_6N_2O$	110.1	0.52
45.	9.74	Benzene, [(1,1-dimethylethyl)thio]-	$C_{11}H_{16}S$	166.2	0.40
46.	9.69	Phenol, 4-butoxy-	$C_{10}H_{14}O_2$	166.2	0.71
47.	9.96	2-Amino-oxazole	$C_3H_4N_2$	84.07	0.78
48.	10.17	4-Amino-5-hydrazino-1,2,4-triazole	$C_2H_6N_6S$	146.1	0.70
49.	10.29	Pentylamine, *N*-acetyl-1-cyano-	$C_8H_{14}N_2O$	154.2	0.49
50.	10.44	4-Acetylocta-1,2-diene	$C_{10}H_{16}O$	152.2	0.49
51.	10.55	Benzene, 1,3,5-trimethoxy-	$C_9H_{12}O_3$	168.1	0.48
52.	10.87	3-Hexen-2-one, 5-methyl-	$C_7H_{12}O$	112.1	0.50
53.	11.16	2*H*-1,2,3,4-Tetrazole-2-acetamide	$C_9H_9N_5O$	203.2	0.52
54.	11.53	Phenol, 2,6-dimethyl-4-nitro-	C_8H_9NO	167.1	0.44
55.	11.92	5-Ethyl-1-nonene	$C_{11}H_{22}$	154.2	0.10
56.	11.97	Octanoic acid	$C_8H_{16}O_2$	144.2	0.10
57.	12.11	Diethyl-phenylsilane	$C_8H_{12}Si$	136.2	0.35
58.	12.19	*trans*-2-Decen-1-ol, methyl ether	$C_{10}H_{20}O$	156.2	0.43
59.	12.88	Cyclohexanepropanal, 2,2-dimethyl	$C_{12}H_{22}O$	182.3	0.16
60.	13.02	5,9-Undecadien-2-one, 6,10-dimethyl	$C_{13}H_{22}O$	194.3	0.16
61.	13.64	4-Ethoxy-3-methoxyphenol	$C_8H_{10}O_2$	138.1	0.81
62.	13.81	3-Hepten-2-one, 7-phenyl-	$C_{13}H_{16}O$	188.2	0.17
63.	14.03	Bicyclo[2.2.2]octan-1-ol, 2-methyl-	$C_9H_{16}O$	140.2	0.88

Table 1 (*Contd.*)

S. no.	Ret/time	Compounds	Chem. formula	Mol. wt. (g mol^{-1})	Area (%)
64.	14.23	Pyrrolo[1,2-*a*]pyrazine-1,4-dione hexahydro-	$C_7H_{10}N_2O_2$	154.1	1.63
65.	14.38	2-Cyclohexen-1-ol, 2,6,6-trimethyl-	$C_9H_{16}O$	140.2	0.18
66.	14.44	1-Methoxy-4,4-dimethyl-cyclohex-2-ene	$C_9H_{16}O$	140.1	0.48
67.	14.99	Thiophene, 2-ethyl-5-propyl-	$C_9H_{14}S$	154.2	1.35
68.	15.10	Cyclohexane, 1,2-diethyl-3-methyl-	$C_{11}H_{22}$	154.2	0.28
69.	15.93	Phenol, 3,5-dimethoxy-, acetate	$C_{10}H_{12}O_2$	164.2	1.22
70.	16.37	2-Methyloctadecan-7,8-diol	$C_{19}H_{40}O_2$	300.5	0.22
71.	17.08	Cyclohexane, 1,1,2-trimethyl-	C_9H_{18}	126.1	1.02
72.	17.19	2-(2-Methyl-acryloyl) cyclohexanone	$C_7H_{12}O$	112.1	0.39
73.	17.54	1,3-Dimethyl-5isobutylcyclohexane	$C_{12}H_{24}$	168.3	0.40
74.	17.84	Octane, 1,8-dibromo-	$C_8H_{16}Br_2$	270.0	0.77
75.	18.66	Cyclohexane, 1,2-diethyl-, *cis*	$C_{10}H_{20}$	140.2	0.56
76.	19.19	3,7-Nonadienoic acid, 4,8-dimethyl	$C_{11}H_{18}O_2$	182.2	0.25
77.	19.25	Cyclohexane, 1,1,3,5-tetramethyl	$C_{10}H_{20}$	140.2	0.50
78.	19.60	3-Heptene, 2,2,3,5,6-pentamethyl-	$C_{12}H_{24}$	168.3	0.44
79.	20.00	Cyclohexane, 1,2-diethyl-3-methyl-	$C_{11}H_{22}$	154.2	2.42
80.	20.14	Cyclohexane, 1-ethyl-2-propyl-	$C_{11}H_{22}$	154.1	0.99
81.	20.54	α-Benzylsuccinic acid	$C_{11}H_{12}O_4$	208.2	5.29
82.	20.70	4,4,7-Trimethyl-oct-5-enal	$C_{11}H_{20}O$	168.2	1.29
83.	21.06	1-Hexacosanol	$C_{26}H_{54}O$	382.7	0.37
84.	21.52	1,1′-Bicyclohexyl, 2-propyl-, *cis*	$C_{15}H_{28}$	208.3	0.57
85.	21.60	Benzo[h]quinoline, 2,4-dimethyl-	$C_{15}H_{13}N$	207.2	1.45
86.	22.06	9-Oxabicyclo[6.1.0]nonane,1methyl	$C_9H_{16}O$	140.2	0.73
87.	22.21	3-Phenyl-1-propanol, acetate	$C_{11}H_{14}O_2$	178.2	1.42
88.	22.38	1,2-Dihydro-3-phenylnaphthalene	$C_{16}H_{14}$	206.2	0.64
89.	22.60	Triallylsilane	$C_6H_{15}S$	116.2	0.29
90.	23.51	Benzene, 1-methyl-4-(1-propynyl)-	$C_{10}H_{10}$	130.1	3.53
91.	23.86	Cyclopentane, 1,2-dibutyl-	$C_{13}H_{26}$	182.3	0.63

pentamethyl-). The main aromatics identified are benzene-D6, phenol, 1,3-benzenediamine (4-methyl-), phenol (2-methoxy-), 1,2-benzenediol (3-methoxy-), 2-methoxy-4-vinylphenol, benzene ([[(1,1-dimethylethyl)thio]-), phenol (4-butoxy-), benzene (1,3,5-trimethoxy-), phenol (2,6-dimethyl-4-nitro-), and benzene (1-methyl-4-(1-propynyl)-). The main alcohols detected are, 1,2,3-propanetriol (1-acetate), 2-cyclohexen-1-ol (2,6,6-tri-methyl-), and bicyclo[2.2.2]octan-1-ol (2-methyl-). The main acids found include isocrotonic acid, propanoic acid (2-(hydroxyimino)), 3,7-nonadienoic acid (4,8-dimethyl), α-ben-zylsuccinic acid, and octanoic acid. Other notable components detected are 1*H*-pyrazole (1,3-dimethyl-), cyclohexane (1-ethyl-2-propyl-), tetramethylammonium perchlorate, acetamide, *N*,*N*-dimethylacetamide, urea (trimethyl-), methyl isobutyl ketone, piperazine (1-methyl-), oxirane (2-methyl-2-pentyl-), 2-vinyl-furan, formic acid phenyl ester, 2,4-dimethyl-2-oxazoline-4-methanol, 5-amino-3-methyl-1,2,4-oxadiazole, diethyl-phenylsilane, 1-hexacosanol, and triallylsilane.

The impregnation of nickel on zeolite Y, hydrogen increased the catalytic activity on biomass, as it resulted in maximum production of aromatic hydrocarbons, benzene derivatives, phenols, alcohols and numerous acids. The most prevalent component was benzyl succinic acid ($C_{11}H_{12}O_4$), which had a retention time of 20.54 minutes and an area percentage of 5.29%. 1-Methyl-4-(1-propynyl)-benzene ($C_{10}H_{10}$) was the second prominent compound, with a retention time of 23.51 minutes and an area percentage of 3.53%. The third most

abundant component was 2-methoxy-phenol (C_7H_8O), which had a 3.15% area percentage and a retention time of 5.81 minutes. These observations are in consonant with prior research.

Nisar *et al.*,[41] analyzed the bio-oil recovered from the decomposition of cobalt impregnated sesame biomass and observed the abundance of compounds such as methanol, 1-heptanol-2,4-diethyl, 2-propanone, 5-eicosene, 2-propanone-1-hydroxy, 2-pentanon-1-heptene, 1-decanol-2-hexyl, 1-dodecanol-2-hexyl, nonadecyl trifluoroacetate, and 1-hex-adecanesulfonyl chloride. The compounds found in the oil possessed properties to be used as an energy source; however, upgrading bio-oil was required to remove the oxygen content. Arias *et al.*,[42] investigated rapid catalytic decomposition of vegetable oil waste utilizing metal impregnated catalysts. The findings demonstrated that the combination of acidic and metallic characteristics produced the highest percentages of hydrocarbons that are extremely fuel selective. The metal-loaded catalyst was selective in the production of gasoline-range alkanes, polyenes, ketones, and aromatics (C_3–C_{10}). Nisar *et al.*,[43] performed thermo-catalytic pyrolysis of sesame stalk with Ni–Co loaded MCM-41 and studied the composition of pyrolytic oil by GC/MS, which indicated the presence of furan, phenols, ketones, and aldehydes with different acid compounds. The addition of maltol, phenol, and furfural considerably increased the oil's quality. Aromatic hydrocarbons were also discovered in the oil. Yet in another study Nisar *et al.*[44]

probed the catalytic degradation of almond shells with zinc oxide. The resulting liquid fraction was examined, and the most abundant chemicals in the oil were found to be acetic acid, ethanol, 9-octadecenoic acid, methyl ester, and 1-hydroxy-2-butanone. Furthermore, zinc oxide was observed to proliferate the amount of bio-oil.

3.5. Thermogravimetric analysis and kinetic study

Fig. 7 and Table 2 show the TG/DTG profile of cotton seed press cake at 15 °C min^{-1}. Water evaporation is responsible for the first weight loss from 40 to 95 °C. Hemicellulose degradation is represented by the second weight loss from 220 to 270 °C with a T_{max} of 246 °C. The third weight loss (290–350 °C) with a T_{max} of 324 °C is due to cellulose decomposition, while the last weight loss (390–470 °C) with a T_{max} of 430 °C is due to lignin degradation.

For the kinetic study, the biomass sample impregnated with catalyst was studied at heating rates of 5, 10, 15 and 20 °C min^{-1}. The results attained from these experiments were then used for determining kinetic parameters employing Kissinger equation (eqn (1)). Activation energy, frequency factor and correlation coefficient were determined which are shown in Table 3 and kinetic plot is depicted in Fig. 8. These observations are in line with literature. Using the Kissinger approach, Nisar
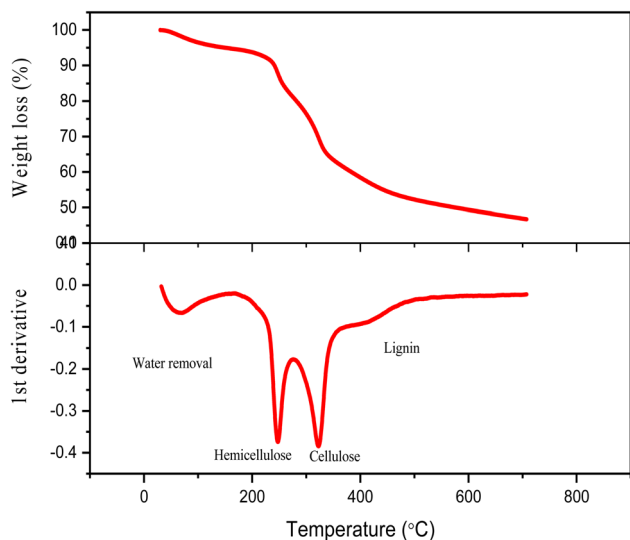
Fig. 7 TG/DTG profile of cotton seed press cake over nickel loaded zeolite Y, hydrogen.

Table 2 Thermogravimetric analysis of cotton seed press cake over nickel loaded zeolite Y, hydrogen at 15 °C min^{-1}

Region	Temp. range (°C)	T_{max} (°C)	Component
I	40–95	65	Water vapours
II	220–270	246	Hemicellulose
III	290–350	324	Cellulose
IV	390–470	430	Lignin

Table 3 Kinetics parameter calculated from catalytic degradation reaction of cotton seed press cake using Kissinger equation

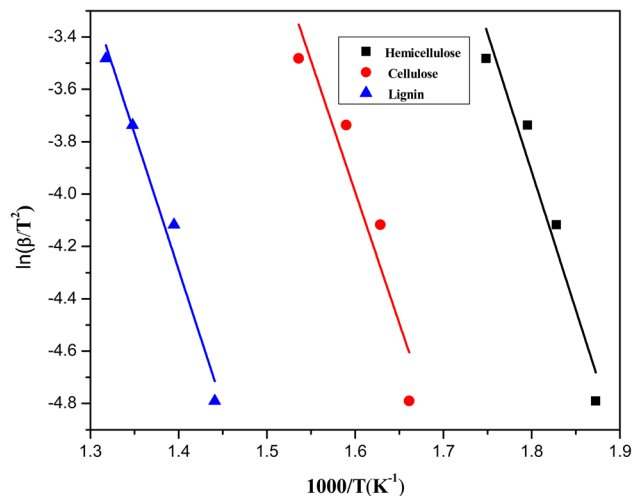| Components	E_a (kJ mol^{-1})	A (min^{-1})	R^2
Hemicellulose	83.14	1.9×10^7	0.921
Cellulose	99.77	1.0×10^8	0.843
Lignin	124.71	1.0×10^{10}	0.965

Fig. 8 Kissinger plot constructed from thermocatalytic decomposition of cotton seed press cake.

et al.[45] examined the pyrolysis of sugarcane bagasse and the activation energy values for the catalyzed reaction were calculated 83.14 kJ mol^{-1}, 99.76 kJ mol^{-1}, and 116.39 kJ mol^{-1} for hemicellulose, cellulose and lignin. In contrast, the Ea for the non-catalytic reaction were 99.76 kJ mol^{-1}, 133.02 kJ mol^{-1}, and 232.79 kJ mol^{-1} for hemicellulose, cellulose and lignin respectively. These findings suggest that the catalyst has reduced the activation energy of biomass degradation reaction.

4. Conclusions

Cotton seed press cake loaded with Ni-doped zeolite Y, hydrogen was decomposed using a locally built pyrolysis equipment to investigate the influence of time, temperature, and catalyst on the yield of pyrolytic products/bio-oil. Kissinger equation was employed to assess kinetic parameters employing Thermogravimetric data. The activation energies for hemicellulose, cellulose, and lignin were found to be 83.14 kJ mol^{-1}, 99.77 kJ mol^{-1} and 124.71 kJ mol^{-1} respectively, in the presence of Ni-doped zeolite Y, hydrogen catalyst. For pyrolysis trials, 300 °C, 20 minutes, and 5% Ni-doped zeolite Y were shown to be the best temperature, duration, and catalyst concentration for producing maximum bio-oil yield (35%). A GC-MS examination of the bio-oil produced under optimum conditions revealed that it is a mixture of aliphatic and aromatic hydrocarbons, phenols and alcohols, some of which have properties appropriate for usage as fuel. Based on the kinetics and pyrolysis results, it was

determined that cotton seed press cake waste shows promise as a possible pyrolysis feedstock for large-scale biofuel production.

Data availability

The authors declare that the data are available in this manuscript and ESI† document in the form of tables and figures.

Author contributions

Marrij Afraz: investigation, methodology, writing – original draft. Jan Nisar: conceptualization, funding acquisition, resources, project administration. Afzal Shah: drafting, review and editing. Ghulam Ali: writing, results and analysis. Faisal Muhammad: review and editing. Farooq Anwar: review and editing. Wan Azlina Wan Abdul Karim Ghani: editing and visualization.

Conflicts of interest

The authors have no conflicts of interest to declare.

Acknowledgements

References

1 J. N. Waqas Ahmad, F. Anwar and F. Muhammad, Future prospects of biomass waste as renewable source of energy in Pakistan: A mini review, *Bioresour. Technol. Rep.*, 2023, 101658.

2 C. Furlan and C. Mortarino, Forecasting the impact of renewable energies in competition with non-renewable sources, *Renewable Sustainable Energy Rev.*, 2018, **81**, 1879–1886.

3 X. Chen, *et al.*, Diesel production via standalone and co-hydrotreating of catalytic fast pyrolysis oil, *Energy Adv.*, 2024, **3**(5), 1121–1131.

4 F. G. Calvo-Flores and J. A. Dobado, Lignin as renewable raw material, *ChemSusChem*, 2010, **3**(11), 1227–1235.

5 H. Kawamoto, Lignin pyrolysis reactions, *J. Wood Sci.*, 2017, **63**(2), 117–132.

6 D. Gavrilescu, Energy from biomass in pulp and paper mills, *Environ. Eng. Manag. J.*, 2008, 7(5), 537–546.

7 N. U. Rehman, *et al.*, Production of Bio-Oil from Thermo-Catalytic Decomposition of Pomegranate Peels over a Sulfonated Tea Waste Heterogeneous Catalyst: A Kinetic Investigation, *Energies*, 2023, 16(4), 1908.

8 N. S. Bentsen, C. Felby and B. J. Thorsen, Agricultural residue production and potentials for energy and materials services, *Prog. Energy Combust. Sci.*, 2014, **40**, 59–73.

9 J. Nisar, *et al.*, Thermo-catalytic decomposition of walnut shells waste over cobalt doped cerium oxide: Impact of catalyst on kinetic parameters and composition of bio-oil, *Chem. Eng. Sci.*, 2023, 119355.

10 A. Faaij, Modern biomass conversion technologies, *Mitig. Adapt. Strategies Glob. Change*, 2006, **11**(2), 343–375.

11 J. Nisar, *et al.*, Enhanced bio-oil yield from thermal decomposition of peanut shells using termite hill as the catalyst, *Energies*, 2022, **15**(5), 1891.

12 J. Nisar, *et al.*, Pyrolysis of juice-squeezed grapefruit waste: Effect of nickel oxide on kinetics and bio-oil yield, *Int. J. Environ. Sci. Technol.*, 2022, **19**(10), 10211–10222.

13 E. Apaydin-Varol, *et al.*, Synthetic fuel production from cottonseed: fast pyrolysis and a TGA/FT-IR/MS study, *J. Anal. Appl. Pyrolysis*, 2014, **105**, 83–90.

14 M. Afraz, *et al.*, Production of value added products from biomass waste by pyrolysis: An updated review, *Waste Manage. Bull.*, 2024, **1**(4), 30–40.

15 B. Babu, Biomass pyrolysis: a state-of-the-art review, *Biofuels, Bioprod. Biorefin.*, 2008, **2**(5), 393–414.

16 A. Galadima and O. Muraza, In situ fast pyrolysis of biomass with zeolite catalysts for bioaromatics/gasoline production: a review, *Energy Convers. Manage.*, 2015, **105**, 338–354.

17 Q.-F. Lin, *et al.*, A stable aluminosilicate zeolite with intersecting three-dimensional extra-large pores, *Science*, 2021, **374**(6575), 1605–1608.

18 J. Li, *et al.*, A 3D extra-large-pore zeolite enabled by 1D-to-3D topotactic condensation of a chain silicate, *Science*, 2023, **379**(6629), 283–287.

19 Z. R. Gao, *et al.*, Interchain-expanded extra-large-pore zeolites, *Nature*, 2024, **628**(8006), 99–103.

20 T. Ennaert, *et al.*, Potential and challenges of zeolite chemistry in the catalytic conversion of biomass, *Chem. Soc. Rev.*, 2016, **45**(3), 584–611.

21 S. Van Donk, *et al.*, Generation, characterization, and impact of mesopores in zeolite catalysts, *Catal. Rev.*, 2003, **45**(2), 297–319.

22 W. B. Widayatno, *et al.*, Upgrading of bio-oil from biomass pyrolysis over Cu-modified β-zeolite catalyst with high selectivity and stability, *Appl. Catal., B*, 2016, **186**, 166–172.

23 A. Abdullah, *et al.*, Potential for sustainable utilisation of agricultural residues for bioenergy production in Pakistan: An overview, *J. Cleaner Prod.*, 2021, **287**, 125047.

24 M. Zerihun and H. Berhe, Physicochemical properties of Cotton seeds oil and its comparison with released and improved cotton varieties in Ethiopia, *Acad. Res. J. Agri. Sci. Res.*, 2018, **6**(7), 443–452.

25 T. H. Malik and M. Z. Ahsan, Review of the cotton market in Pakistan and its future prospects, *OCL*, 2016, **23**(6), D606.

26 G. Ali, *et al.*, Production of Fuel Range Hydrocarbons from Pyrolysis of Lignin over Zeolite Y, Hydrogen, *Energies*, 2022, **16**(1), 215.

27 R. L. Blaine and H. E. Kissinger, Homer Kissinger and the Kissinger equation, *Thermochim. Acta*, 2012, **540**, 1–6.

28 F. Xu, *et al.*, A novel Ni-doped micro-mesoporous Y zeolite for high efficiency denitrogenation, *J. Porous Mater.*, 2022, 1–13.

29 M. N. Uddin, W. W. Daud and H. F. Abbas, Co-production of hydrogen and carbon nanofibers from methane decomposition over zeolite Y supported Ni catalysts, *Energy Convers. Manage.*, 2015, **90**, 218–229.

30 M. Kalhor and Z. Zarnegar, 1-Methylimidazolium ionic liquid supported on Ni@ zeolite-Y: fabrication and performance as a novel multi-functional nanocatalyst for one-pot synthesis of 2-aminothiazoles and 2-aryl benzimidazoles, *Res. Chem. Intermed.*, 2022, **48**(2), 519–540.

31 M. Kalhor, S. Banibairami and S. A. Mirshokraie, Ni@ zeolite-Y nanoporous; a valuable and efficient nanocatalyst for the synthesis of N-benzimidazole-1, 3-thiazolidinones, *Green Chem. Lett. Rev.*, 2018, **11**(3), 334–344.

32 R. Malyala, *et al.*, Activity, selectivity and stability of Ni and bimetallic Ni–Pt supported on zeolite Y catalysts for hydrogenation of acetophenone and its substituted derivatives, *Appl. Catal., A*, 2000, **193**(1–2), 71–86.

33 R. Philipus, *et al.*, Comparative study of photocatalytic activity of Ni-doped ZnO and zeolite supported Ni-doped ZnO prepared by co-precipitation method, in *Materials Science Forum*, Trans Tech Publications, 2015.

34 K. Thirugnanasambandham and V. Sivakumar, An eco-friendly approach for copper (II) ion adsorption onto cotton seed cake and its characterization: Simulation and validation, *J. Taiwan Inst. Chem. Eng.*, 2015, **50**, 198–204.

35 Z. He, *et al.*, Surface characterization of cottonseed meal products by SEM, SEM-EDS, XRD and XPS analysis, *J. Mater. Sci. Res.*, 2018, **7**(1), 28–40.

36 M. Kaewpanha, *et al.*, Steam reforming of tar derived from the steam pyrolysis of biomass over metal catalyst supported on zeolite, *J. Taiwan Inst. Chem. Eng.*, 2013, **44**(6), 1022–1026.

37 M. Siva Sankari, *et al.*, Oil Cakes as Sustainable Agro-Industrial Feedstock for Biocarbon Materials, *ChemBioEng Rev.*, 2022, **9**(1), 21–41.

38 V. Volli and R. Singh, Production of bio-oil from mahua de-oiled cake by thermal pyrolysis, *J. Renewable Sustainable Energy*, 2012, **4**(1), 013101.

39 J. F. Gonzalez, *et al.*, Pyrolysis of almond shells. Energy applications of fractions, *Ind. Eng. Chem. Res.*, 2005, **44**(9), 3003–3012.

40 F. Muhammad, *et al.*, Improved bio-oil yield from thermo-catalytic pyrolysis of Citrus limetta waste over pumice: Determination of kinetic parameters using Kissinger method, *Bioresour. Technol. Rep.*, 2023, **24**, 101635.

41 J. Nisar, *et al.*, Kinetics of the pyrolysis of cobalt-impregnated sesame stalk biomass, *Biomass Convers. Biorefin.*, 2020, **10**, 1179–1187.

42 S. Arias, *et al.*, Hydrogen-free deoxygenation of industrial vegetable oil waste using Ce, Zr-NiAl catalysts for second-generation biofuels production, *Mol. Catal.*, 2022, **529**, 112554.

43 J. Nisar, *et al.*, Thermocatalytic decomposition of sesame waste biomass over Ni-Co-doped MCM-41: kinetics and physicochemical properties of the bio-oil, *Energies*, 2023, **16**(9), 3731.

44 J. Nisar, *et al.*, Pyrolysis of almond shells waste: effect of zinc oxide on kinetics and product distribution, *Biomass Convers. Biorefin.*, 2022, **12**, 2583–2595.

45 J. Nisar, *et al.*, Kinetics of pyrolysis of sugarcane bagasse: effect of catalyst on activation energy and yield of pyrolysis products, *Cellulose*, 2021, **28**(12), 7593–7607.